Thin-film piezoelectric MEMS

Chang-Beom Eom and Susan Trolier-McKinstry, Guest Editors

Major challenges have emerged as microelectromechanical systems (MEMS) move to smaller size and increased integration density, while requiring fast response and large motions. Continued scaling to nanoelectromechanical systems (NEMS) requires revolutionary advances in actuators, sensors, and transducers. MEMS and NEMS utilizing piezoelectric thin films provide the required large linear forces with fast actuation at small drive voltages. This, in turn, provides accurate displacements at high integration densities, reduces the voltage burden on the integrated control electronics, and decreases NEMS complexity. These advances are enabled by the rapidly growing field of thin-film piezoelectric MEMS, from the development of AlN films for resonator and filter applications, to their implementation in adaptive radio front ends, to the demonstration of large piezoelectricity in epitaxial $Pb(Zr,Ti)O_3$ and $PbMg_{1/3}Nb_{2/3}O_3$–$PbTiO_3$ thin films. Applications of low voltage MEMS/NEMS include transducers for ultrasound medical imaging, robotic insects, inkjet printing, mechanically based logic, and energy harvesting. As described in this article, advances in the field are being driven by and are prompting advances in heterostructure design and theoretical investigations.

Introduction

Piezoelectricity and piezoelectric materials

Piezoelectric materials enable electromechanical transduction. They generate electrical signals in response to applied mechanical stress, with applications ranging from the flashing lights in children's shoes to motion- or vibration-powered wireless sensors. Conversely, piezoelectrics also respond to applied electrical fields by changing shape—for example, piezoelectric transducers are used to generate high-frequency acoustic waves for ultrasound medical imaging (see **Figure 1**) or to enable nanoscale positioning in scanning probe microscopes. More details on the definition of piezoelectricity and the standard notation used to describe it are given in the sidebar.

Bulk piezoelectric materials are widely employed for a diverse range of applications. Figure 1 shows ultrasonic images of a fetus taken using a single piezoelectric piston in the 1960s and by ceramic $Pb(Zr,Ti)O_3$ (PZT) two-dimensional (2D) transducer arrays. The improved image quality in modern ultrasonic imaging systems and the capability of three-dimensional (3D) rendering were enabled by the development of more sensitive, broader bandwidth, higher frequency piezoelectric transducer arrays. The last 15 years have seen an explosion in the development of new piezoelectric single crystals[1] and lead-free piezoelectric materials,[2] resulting in large improvements in material property coefficients and new application areas.

Thin films and multilayered heterostructures of piezoelectric materials have great potential for micro- and nanoscale devices due to the added functionality provided by the electromechanical transduction coupled with the ability to micromachine using standard processing tools. Advances in bulk piezoelectric materials have rapidly been incorporated into thin films through the development of improved growth techniques. Moreover, the last decade has seen significant growth in the ability to design and micromachine functional devices. At the same time, foundries are beginning to provide services for piezoelectric films, increasing the breadth of the community able to access such functional materials. This issue of *MRS Bulletin* highlights the integration of next-generation piezoelectric thin films into micromechanical systems (MEMS) and nanoelectromechanical systems (NEMS).

Piezoelectric MEMS overview

Numerous means of generating motion in micromachined structures have been reported, including electrostatic, magnetostrictive, thermal, and piezoelectric approaches. State-of-the-art MEMS devices often use silicon, SiO_2, Si_xN_y, SiC, or diamond-like carbon micro- and nanomechanical structures actuated by electrostatic forces, which exist between charged surfaces at a distance.[3–7] This technology has opened many new application possibilities, for example, in the area of MEMS spatial light modulators being

Chang-Beom Eom, Department of Materials Science and Engineering, University of Wisconsin–Madison; eom@engr.wisc.edu
Susan Trolier-McKinstry, Pennsylvania State University; STMcKinstry@psu.edu
DOI: 10.1557/mrs.2012.273

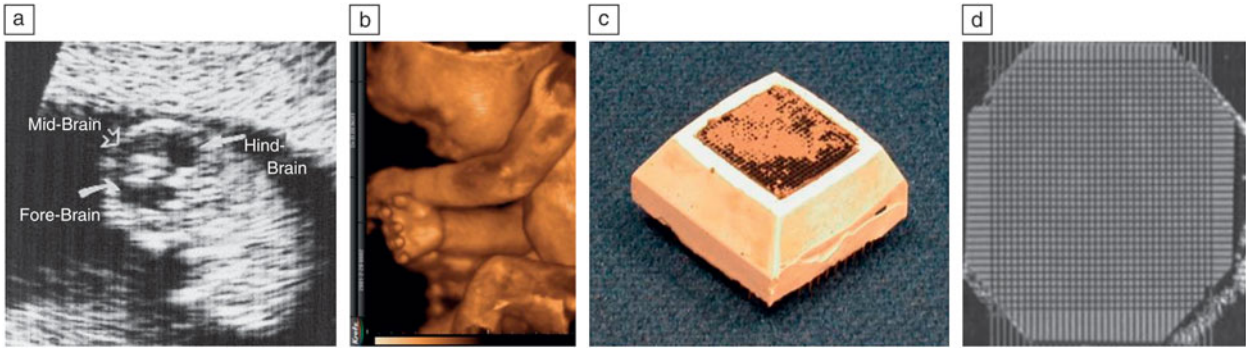

Figure 1. Ultrasound images of a fetus taken by (a) a single piezoelectric piston in 1960 and (b) 3D image scans using ceramic PZT 2D transducer arrays at 1 MHz. (Image courtesy of GE Medical.) (c) PZT ceramic 20 × 20 = 400 element 1-MHz 2D array, (d) 256 × 256 = 65,536 5-MHz subdiced elements. (Image courtesy of Stephen Smith at Duke University.) Both transducer arrays are about 1 inch on a side. The quality of images depends on the piezoelectric and mechanical coupling coefficients and the bandwidth.

Definitions of piezoelectricity

Piezoelectricity is the linear coupling between polarization (P_i) and an applied strain (x_{ij}) or stress (σ_{ij}). For the direct piezoelectric effect, using standard Einstein notation (where the subscripts *ijk* are integers from 1 to 3):

$$P_i = d_{ijk}\sigma_{jk}$$

$$P_i = e_{ijk}x_{jk}.$$

Both d_{ijk} and e_{ijk} are piezoelectric charge coefficients. The converse piezoelectric coefficient yields a mechanical response resulting from an applied electric field:

$$x_{ij} = d_{kij}E_k$$

$$\sigma_{ij} = e_{kij}E_k.$$

As a result, piezoelectric materials can be used either as strain/stress sensors or as actuators in which displacement is induced by an applied electric field (E_k). Often, in describing these devices, a contracted matrix notation is utilized, where a single index running from 1–6 is used for the stress or strain. In thin films, the mechanical boundary conditions differ from unconstrained bulk materials in that the strains are typically known in-plane, while out-of-the-substrate-plane, the film is stress free. Thus, effective coefficients, $d_{ijk,f}$ or $e_{ijk,f}$ are widely employed.

developed for maskless lithography.[8,9] MEMS devices are continually pushed in the direction of smaller size and increased integration density with increased speed, larger range of motion, and more powerful actuating elements. Currently this is accomplished by incorporating passive mechanical elements of nanoscale dimensions within larger MEMS devices driven electrostatically.

In comparison to electrostatic devices, piezoelectric MEMS possess a number of key characteristics that make them attractive:[10]

1. High frequency, temperature-stable resonant devices can be prepared with excellent temperature and frequency stability.[11,12] This is achievable by the deposition of wurtzite-structured films on either mechanically released structures or acoustic Bragg gratings. This technology is now ubiquitous in high frequency filters (e.g., for cellular telephones) and enables significant miniaturization of handsets.[13,14] In devices based on AlN, the processing is complementary metal oxide semiconductor (CMOS)-compatible, enabling far more complex sensing and communication circuits. Details are given in the article by Piazza et al. in this issue.
2. Piezoelectric charges develop whenever the device undergoes mechanical excitation. As a result, piezoelectric sensors can operate *without applied power* (although the remainder of the electronics may well require a power source). The net result is that low-power devices with low noise floors and broad dynamic ranges are possible.
3. The coupling between mechanical and electrical energies means that piezoelectric MEMS are also of interest for energy harvesting applications, when they can be mounted on vibrating structures.[15–18] Thus, small vibrations can produce power. Although the harvesting levels tend to be modest, they are of interest for low power wireless sensor nodes. Moreover, it is possible that piezoelectric MEMS devices could be used to power body-worn sensor networks. For example, in body-worn devices, Yun et al.[19] demonstrated accelerations at a few Hz, which ranged from ~5–15 m/s^2, depending on the location, due to human motion. Much larger accelerations occur during the heel strike in normal walking (>50 m/s^2).[20] Von Buren showed that the maximum

https://doi.org/10.1557/mrs.2012.273 Published online by Cambridge University Press

power density for energy harvesting from a human walking at 4 km/h is ~2.1 mW/cm^3.[21] All of these motions provide the possibility of generating low levels of power. Likewise, it was recently demonstrated that larger piezoelectric devices can harvest enough energy from the motion of the heart to power pacemakers under a wide variety of conditions.[22]

4. Piezoelectric actuators have substantially higher energy densities than electrostatic actuators. For actuators, the force per unit area increases linearly with the electric field, E [$\sim e_{31}E$] for the piezoelectric drive (where e_{31} is the piezoelectric coefficient) and quadratically [$\sim\varepsilon_0\varepsilon_r E^2$] (where ε_0 and ε_r are the permittivity of free space and the relative permittivity, respectively) for the electrostatic approach. Moreover, the permittivity of piezoelectric films exceeds that of air by factors of ~10–1000.[10] As a result, the required driving voltages to achieve a given displacement in structures of the same stiffness typically drop by at least an order of magnitude for piezoelectric actuators. This is critical in enabling actuators that can be driven by CMOS electronics, without requiring energetically expensive charge or voltage pumps.
5. Piezoelectricity scales well as an actuator technology. Provided orientation control can be achieved in the initial layers of a deposited film, AlN and other wurtzite-structured compounds should show essentially bulk piezoelectric response down to very small size scales (in the tens of nm range). Likewise, it has been demonstrated that ferroelectricity (and hence piezoelectric activity, which occurs in all ferroelectric materials) can be retained in films of only a few unit cells in thickness.[23] Furthermore, the energy density of the piezoelectric actuator also scales well with decreasing dimensions so that useful work can be done even with small volume structures. This decreases the complexity, enables higher integration density, and, as discussed previously, reduces the voltage burden on the integrated control electronics. In addition, robustness comes from the fact that high electric fields are confined inside solid-state material(s).

Given these features, the field of piezoelectric MEMS has burgeoned over the past decade, with significant progress being made both in achievable materials response and in commercialization of devices.[24–31] Manufacturing of piezoelectric MEMS has also benefitted tremendously from the infrastructure and equipment developments resulting from ferroelectric memories.[32,33] This issue of *MRS Bulletin* is designed to introduce readers to the current state of research in thin-film piezo MEMS/NEMS applications for electronic, mechanical, and energy applications. The issue contains six articles from leading research groups focusing on perovskite and AlN based piezoelectric thin films and their applications in MEMS. This introductory article describes the piezoelectric materials in most common use, recent advances in piezoelectric thin-film growth, and reviews the length scales over which piezoelectric MEMS are currently being explored.

Key materials for piezoelectric MEMS

Among the important properties of materials for piezoelectric devices are the piezoelectric coefficients, the ferroelectric transition temperature, and the stability of the piezoelectric response.

Two principal crystal structures are in use for piezoelectric MEMS: the wurtzite and perovskite structures. The wurtzite structure, shown in **Figure 2**, is adopted by both ZnO and AlN. All of the atoms are tetrahedrally coordinated and are arranged in puckered hexagonal rings perpendicular to the crystallographic *c*-axis. In a single crystal, all of the cation polyhedra are arranged in the same orientation. On application of a stress parallel to the *c*-axis, the tetrahedra deform primarily by changing the N–Al–N bond angle, rather than changing the Al–N bond length. This produces a relative displacement of the center of the positive and negative charges within the unit, which is the origin of the piezoelectric d_{33} coefficient in AlN.

It is essential to recognize that the piezoelectric coefficient in AlN depends on the orientation of the crystallites as prepared. Reorientation of the polarization would require breaking primary chemical bonds, so AlN is not ferroelectric. This is useful from the perspective that it yields piezoelectric constants that are very stable as a function of temperature, frequency, and the amplitude of the drive electric field. These attributes are exploited in thin-film bulk acoustic resonators, as described in the article by Piazza et al. in this issue.

The perovskite structure in **Figure 3** shows some of the more common ferroelectric distortions (exaggerated for clarity). In most perovskites, the unit cell elongates parallel to the direction of the spontaneous polarization and contracts laterally. These materials are ferroelectric below the Curie temperature

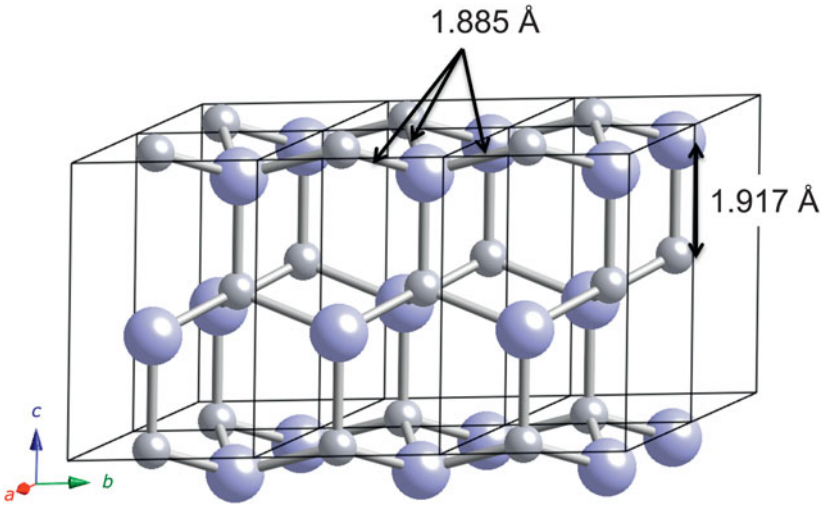

Figure 2. Wurtzite crystal structure of AlN showing Al atoms in gray and N in blue. All Al-centered tetrahedra are arranged with one neighbor directly above (parallel to the *c*-axis) and three neighbors forming the base of a pyramid below.

https://doi.org/10.1557/mrs.2012.273 Published online by Cambridge University Press

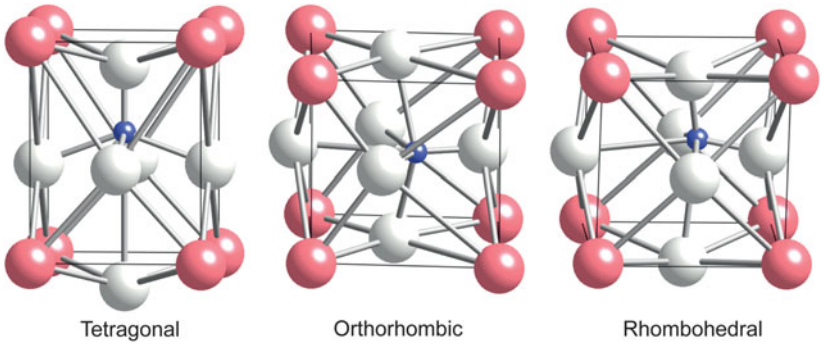

Figure 3. Typical ferroelectric distortions (exaggerated for clarity) of the perovskite ABO_3 structure; the A ions (red) are at the corners of the unit cell, the B ions (blue) are close to the center of the unit cell, and the O ions (white) are near the face centers. Upon developing spontaneous polarization, a spontaneous strain also develops.

and typically possess a residual domain structure, which is a function of the local electrical and mechanical fields in the film. Piezoelectric properties in perovskites are generally optimized when the material is poised on the brink of a structural instability (e.g., at a phase transition).[34] Morphotropic phase boundaries (temperature-independent boundaries between phases of different compositions, abbreviated as MPBs) are particularly useful, as the polarizability and properties are enhanced over a wide range of temperatures. This prompts the use of solid solution systems with morphotropic phase boundaries such as $PbZr_{1-x}Ti_xO_3$ (PZT) and $PbMg_{1/3}Nb_{2/3}O_3$–$PbTiO_3$ (PMN-PT). Recent work on superior piezoelectric responses in perovskite thin-film materials is reviewed in the articles by Baek et al. and Funakubo et al. in this issue.

In perovskite ferroelectrics, there are multiple mechanisms available to contribute to the piezoelectric constants, including polarization extension, polarization rotation, and domain wall motion, as illustrated in **Figure 4**.[35–37] For example, polarization extension entails a change in the shape of the unit cell. In materials such as PZT, the cell elongates parallel to the polarization direction when the electric field is applied in the same direction. This contributes to the *intrinsic* piezoelectric response. In contrast, domain wall motion produces a shape change via a combination of local reorientation of the spontaneous strain (the strain that develops with the polarization) and changes in the degree of clamping imposed by the surrounding grains/domains.[38] Finally, polarization rotation is associated with rotation of the polarization away from its zero field orientation due to application of an applied electric field. In general, the crystallographic anisotropy that holds the polarization in a particular orientation is larger than typical magnetocrystalline anisotropies. This typically results in narrow domain walls in ferroelectric materials. However, when there is an adjacent phase transition that lowers the energy barrier between different ferroelectric distortions, the polarization can rotate from its preferred direction during application of an electric field. This can produce large strains, particularly in the case of domain-engineered perovskite single crystals such as [001]-oriented rhombohedral PMN-PT where the applied electric field can induce polarization rotation without significant domain wall motion.[1]

Several different piezoelectric coefficients are in use in MEMS devices, as shown in **Figure 5**. In piezoelectric MEMS, the longitudinal piezoelectric coefficient ($d_{33,f}$—here as elsewhere in this issue, the subscript f after a piezoelectric coefficient denotes an effective coefficient for a thin film) can be utilized if a film electroded on the top and bottom surfaces is strained in the thickness direction. Since the film thickness is small, the surface displacement generated is modest but potentially useful in some electronics applications, as detailed in the article by Newns et al. in this issue. Alternatively, $d_{33,f}$ can also

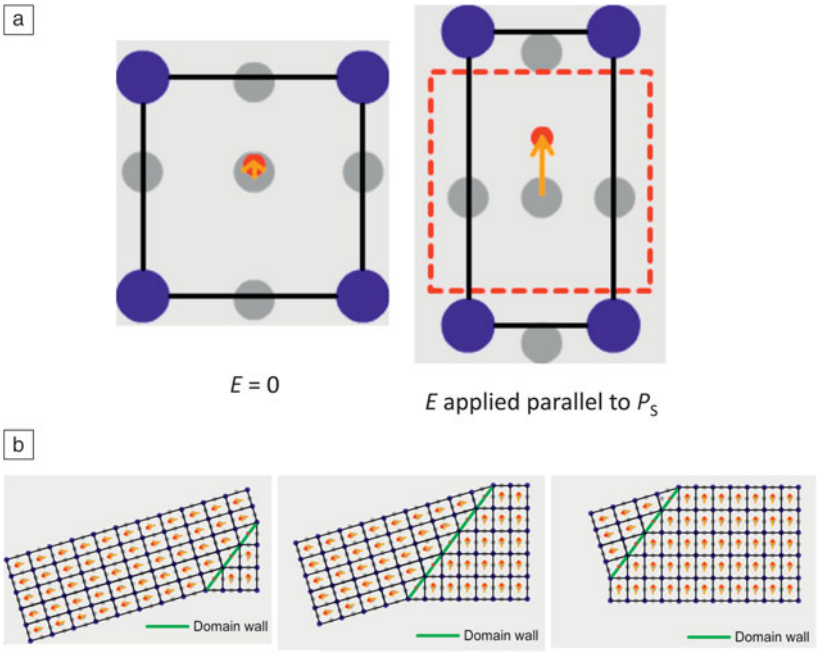

Figure 4. Illustrations (with distortions exaggerated to simplify visualization) of different mechanisms for piezoelectricity. (a) Extension of a perovskite unit cell. View looking along the *a*-axis of a perovskite material with tetragonal distortion. The blue atoms at the corners of the unit cell correspond to large cations such as Pb; O is shown in gray; and the small B site cation (typically Ti, Zr, or Nb) is shown in red. The arrow shows the orientation of the spontaneous polarization, P_S. The black box outlines the unit cell. Distortion of the unit cell from its original shape (shown in the red dotted outline) is apparent on application of an electric field, *E*. (b) Motion of a domain wall in a tetragonally distorted perovskite, in which the directions of the spontaneous polarization differ by 90°. As the domain wall moves, the material changes shape. Figure courtesy of I. Fuji.

https://doi.org/10.1557/mrs.2012.273 Published online by Cambridge University Press

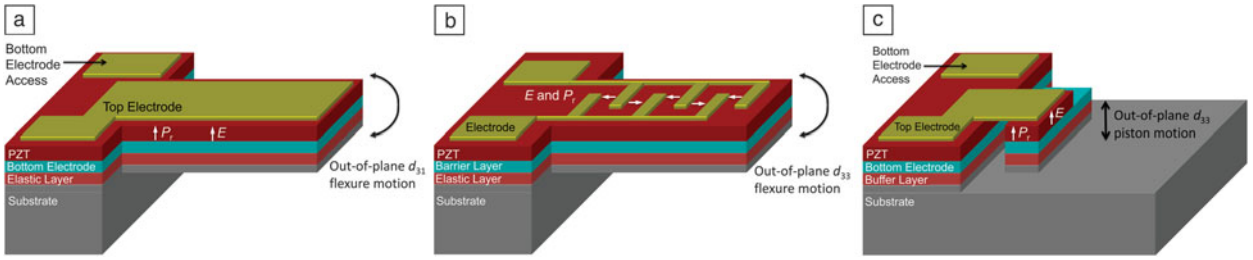

Figure 5. Illustration of common sensing and actuation modes in piezoelectric microelectromechanical systems. (a) Bending mode induced by $e_{31,f}$ (sometimes called d_{31} mode) for a film with top and bottom electrodes. The unimorph structure bends when lateral contraction of the piezoelectric layer acts on the passive elastic layer. (b) Out-of-plane bending due to in-plane expansion of d_{33} actuated-structure using interdigitated electrodes. In order to confine the electric field in the plane of the device, the layers underneath the piezoelectric should be electrically insulating. Barrier layers such as ZrO_2 or HfO_2 are typically required to prevent reaction between lead-based perovskites and Si or SiO_2 elastic layers. (c) Piston motion due to the out-of-plane d_{33} coefficient. Note: PZT, $Pb(Zr,Ti)O_3$; E, electric field; P_r, remanent polarization.

be employed if a ferroelectric film is deposited on an insulating substrate, and interdigitated electrodes (IDE) are patterned on the film surface. In this case, the remanent polarization can be induced in the plane of the film between the electrode fingers; on actuation with an electric field, the $d_{33,f}$ constant produces a strain in the plane of the film. When a flexural structure is prepared, where the piezoelectric layer and its electrodes are stacked with a passive elastic layer, modest in-plane strains can produce large out-of-plane deflections, as shown in Figure 5.[39,40] This IDE geometry is also widely adopted in piezoelectric energy harvesting devices, as described in the article by Kim et al. in this issue. An alternative approach to achieving large deflections with thin films is to use the effective transverse piezoelectric coefficient ($e_{31,f}$) of the material such that a film electrode on the major surfaces is used to flex a unimorph structure with a passive elastic layer.

Growth and integration of piezoelectric thin films

Piezoelectric thin films are essential to realize highly integrated piezoelectric MEMS devices. The last decade has seen significant advances in the growth of uniform, high-response thin films.[14] For example, for AlN, growth of highly textured films with well-defined thicknesses across large-area wafers is now realized at the industrial level. Similarly, growth of high-quality polycrystalline, textured, and epitaxial perovskite films with complex chemistries is becoming increasingly routine.[10,41–45] Lu et al. demonstrated significant polarization retention enhancement in ultrathin $BaTiO_3$ by introducing a 2 unit cell $SrTiO_3$ layer between the $BaTiO_3$ and $SrRuO_3$ metallic oxide electrodes to eliminate the unfavorable interface termination.[46] Moreover, in thin films, wherein deposition conditions can be maintained far from equilibrium, metastable phases that cannot be obtained by quenching of bulk materials can be generated. There is great potential for the discovery of new phases by using vapor phase deposition methods in creative ways.[47] Furthermore, it is possible to grow artificially layered multilayer structures[48,49] and to control film orientations.[50]

Incorporation of piezoelectric materials such as PZT and PMN-PT into NEMS and MEMS pushes these materials into size regimes where their behavior can be very different from their bulk properties.[51] Significant progress has been made in the last decade in the fundamental understanding of ferroelectric properties of thin films using thermodynamics. For example, thermodynamic calculations and phase field simulations have suggested that the morphotropic phase boundary in strained PZT thin-film shifts in composition relative to the bulk single crystal.[52] Particularly, with regard to the effect of strain on the ferroelectric transitions and ferroelectric responses of thin films,[53,54] there are many unresolved fundamental questions associated with the roles of boundary conditions, internal defects (point defects, dislocations, and grain boundaries), as well as the size, shape, and spatial arrangement of ferroelectric crystals on the phase transitions, domain structures, and their influence on the response of MEMS structures.

One of the areas that is well understood from a theoretical perspective is the role of strains and substrate clamping on the properties of piezoelectric films.[51,52] Large strains can exist in thin films due to differences in lattice parameters and thermal expansion behavior between the piezoelectric thin films and the underlying substrate, for example. The substrate constrains the electric-field-induced lateral strains in the piezoelectric layer, while in-plane stresses influence both the domain structure and the mobility of domain walls. As a result, the properties of perovskite thin films can be dramatically different from the intrinsic properties of the corresponding unstrained bulk materials. While such strain often leads to degraded film properties, if judicious use is made of substrates and growth parameters, in principle, strain offers the opportunity to enhance particular properties of a chosen material in thin-film form, via strain engineering.[55] Since piezoelectric properties are sensitive to the distortions and volume of the unit cell, epitaxial strain can be used to tailor and enhance their piezoelectric properties, as demonstrated for ferroelectric thin films.[56] The symmetry, three-dimensional strain states and domain structures, and substrate

https://doi.org/10.1557/mrs.2012.273 Published online by Cambridge University Press

clamping of the piezoelectric thin films all play central roles in determining piezoelectric response.

Piezoelectric films

Several review papers are available for the preparation of polycrystalline, oriented, and epitaxial perovskite films.[24–26] **Figure 6** shows a summary of progress in this area. Over the past two decades, the available piezoelectric coefficients for perovskite thin films on Si substrates have increased by an order of magnitude. These improvements have resulted from developing crystallographic texture, improving compositional uniformity, and engineering internal fields in the films such that films are polarized as-grown.

Two of the articles in this issue focus on recent advances in the growth of epitaxial perovskite piezoelectric films. The article by Funakubo et al. reviews work on epitaxial thin films of $PbZr_{1-x}Ti_xO_3$ on Si substrates. The extensive knowledge base on microfabrication on Si, coupled with the large wafer sizes available, makes this substrate particularly critical for manufacturable scale-up of piezoelectric MEMS devices. **Figure 7**a shows an epitaxial $SrTiO_3$ template layer on (001) silicon now widely employed for epitaxial growth of perovskites on Si. Improved piezoelectric properties in epitaxial films result from three areas of continuous advancement: thin-film deposition techniques, development of a high quality epitaxial template on silicon substrate,[57–60] and epitaxial conductive oxide electrodes.[61,62] Physical deposition techniques of choice include sputtering, metalorganic chemical vapor deposition, pulsed laser deposition, or molecular beam epitaxy. In the case of $PbZr_{1-x}Ti_xO_3$, epitaxy not only allows excellent piezoelectric properties, it also enables a platform to study single-crystal-like material properties, which is critical given the low availability of PZT single crystals near the morphotropic phase boundary. In particular, epitaxial piezoelectric thin films with different orientations can be obtained by controlling the orientation of the substrate. Since the properties of perovskite materials are often anisotropic, control of crystalline directions enables a way to control the macroscopic physical response, such as the ferroelectric polarization.

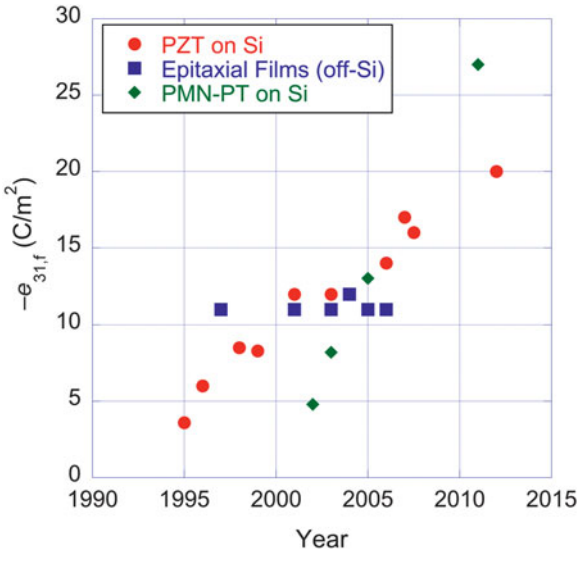

Figure 6. Evolution in piezoelectric $e_{31,f}$ coefficients, showing comparisons to data for bulk PZT materials. Data courtesy of P. Muralt. Adapted from Reference 45. Note: PZT, $Pb(Zr,Ti)O_3$; PMN-PT, $PbMg_{1/3}Nb_{2/3}O_3$–$PbTiO_3$.

Single crystals of materials such as $Pb(Mg_{1/3}Nb_{2/3})O_3$–$PbTiO_3$ (PMN-PT) have been shown to yield giant piezoelectric coefficients (4–5 times higher than conventional polycrystalline piezoelectrics). These single crystals are of great interest for incorporation into active devices, especially medical ultrasound transducers.[1] The giant strains are attributed to electric-field induced polarization rotation and ultimately to a phase transition from rhombohedral to tetragonal in <100> oriented PMN-PT single crystals.[63] In this issue, Baek et al. discuss recent success in the fabrication of PMN-PT based heterostructures with the highest piezoelectric coefficients ever realized on silicon substrates. Figure 7b shows a cross-sectional low magnification bright-field transmission electron microscopy (TEM) image of a PMN-PT/$SrRuO_3$/$SrTiO_3$ epitaxial thin-film heterostructure on a Si substrate. The inset shows the selected-area electron diffraction (SAED) pattern taken from the PMN-PT layer. The high-resolution TEM image (Figure 7c) exhibits an atomically sharp interface between the $SrRuO_3$ and PMN-PT layers; the epitaxial match between the layers is clear. Using an epitaxial $SrTiO_3$ template layer deposited by molecular beam epitaxy[59] and lattice-matched $SrRuO_3$ metallic oxide bottom electrodes, epitaxial PMN-PT films were grown by off-axis sputtering.[64] The large effective transverse ($-e_{31,f}$) piezoelectric coefficients of –27 C/m^2 are the highest values reported for any piezoelectric film and close to those of single crystals.[65]

A simple estimate shows that integrating such piezoelectric films into MEMS is likely to dramatically improve performance in a variety of applications. In their article in this issue, Baek et al. demonstrate that giant piezoelectric coefficient thin films can be successfully integrated into cantilever structures that dramatically outperform electrostatic actuators. Since most common electrostatic actuators use voltage across an air gap and are much softer than piezoelectric ones, for a fair comparison, we consider internal electrostatic actuation.[66] For a typical electrostatic material with Poisson's ratio (ν) = 0.27 and $\varepsilon_r = 9$, a giant piezoelectric coefficient with $e_{31} = -29$ C/m^2 would be equivalent to a dc bias of ≅1.4 MV/μm. Such high biases cannot be achieved in internal electrostatic actuators. The practical way of looking at this is that a force achieved by the intrinsic electrostatic actuator at 100 V requires only 0.01 V in a *hyper*-active NEMS.

Utilizing piezoelectric MEMS over multiple length scales

Adaptive and adjustable optics

Micromachined piezoelectric MEMS range over a wide range of length scales. On the extreme upper end are large-area devices for applications such as adaptive optics for

https://doi.org/10.1557/mrs.2012.273 Published online by Cambridge University Press

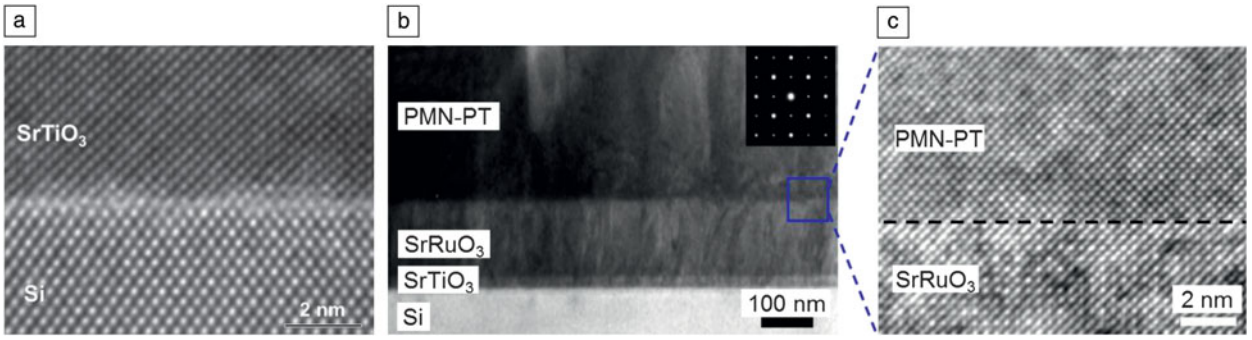

Figure 7. (a) High resolution transmission electron microscope (TEM) image of epitaxial $SrTiO_3$ on silicon grown by molecular beam epitaxy. (Image courtesy of Xiaoqing Pan of the University of Michigan and Darrell Schlom at Cornell University.) $SrRuO_3$ can then be epitaxially grown on top of the $SrTiO_3$ by off-axis sputtering to serve as the templating layer for the piezoelectrics, as well as a bottom electrode. (b) Bright-field cross-sectional TEM image of an epitaxial $PbMg_{1/3}Nb_{2/3}O_3$–$PbTiO_3$ (PMN-PT)/$SrRuO_3$/$SrTiO_3$ thin-film heterostructure on an Si substrate. The inset shows the selective area electron diffraction pattern of the PMN-PT layer along the [100] zone axis showing a single crystal. (c) High-resolution TEM image of PMN-PT and $SrRuO_3$ interface. (b) and (c) are adapted from Reference 65.

telescopes.[67] In this case, the piezoelectric film can be used to produce local deformation of a mirror surface, in order to correct figure errors associated either with fabrication of the component or atmospheric distortion. The ability to prepare a dense array of actuator elements that operate at low voltages is an appealing alternative to the implementation of arrays of bulk electrostrictive actuators.[68,69] Adaptive optics systems incorporating piezoelectric MEMS have been developed for a range of wavelengths, from the visible to the x-ray regime. Telescopes for the latter application provide an example of truly large-area use of adjustable optics. For example, should a mission such as Gen-X (one of the proposed replacements for the Chandra X-ray Observatory) be flown, it would require up to 10,000 m^2 of actuatable optics in order to correct the figures of the nested hyperboloid reflecting segments used to focus the x-rays (see **Figure 8**).[70,71] In this case, the "micro" in "microelectromechanical systems" is clearly a misnomer, although the fabrication techniques would involve conventional micromachining for patterning of the electrodes.

Energy harvesting

Some MEMS energy harvesting systems are also comparatively large (mm–cm length scales). This decreases the resonance frequencies to match those of ambient vibration sources (typically <500 Hz) and maximize the current collection areas (to increase the harvested power). Typical examples are shown in **Figure 9**. Today's wireless sensor networks have an incredible range of applications. They can be used for monitoring factory machinery and social infrastructures, tracking environmental pollution and metropolitan traffic flow, or operating intelligent buildings and bridges. While the potential uses for wireless sensors seem endless, there is one limiting factor: batteries. Despite improvements in microelectronic technology, which have reduced energy consumption, wireless sensors still require batteries, which in turn require replacement, at least periodically. Battery replacement can be a significant task for a large-scale network.

Self-powered electronics, utilizing locally available energy sources, have been a major aspiration for technology developers for a long time. However, this ambition has been impeded by challenges, such as the limitations imposed by fabrication methods, materials, and, most importantly, the magnitude of power required for microelectronic components. Progress made in the last decade on all these fronts—advanced thin-film deposition and MEMS design, better performing piezoelectric materials, and drastic reduction in the power requirement for the microelectronics—may have brought us closer to practically realizing that dream. We expect that very soon it will be possible for a coin-sized harvester to harvest about 100 μW of continuous power at a reasonable cost.

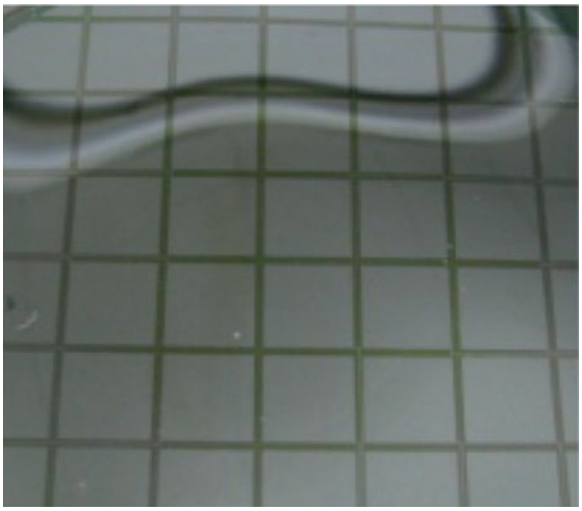

Figure 8. Array of 1 cm^2 piezoelectric cells to adjust the image obtained from a large aperture x-ray space telescope. The sample is a patterned Pt/ $Pb(Zr,Ti)O_3$/Pt/Ti on a glass substrate. It is difficult to see at this scale, but traces run from each cell to the edge of the substrate to facilitate electrical connections. The x-ray reflecting surface is on the opposite side from the piezoelectric actuators.

https://doi.org/10.1557/mrs.2012.273 Published online by Cambridge University Press

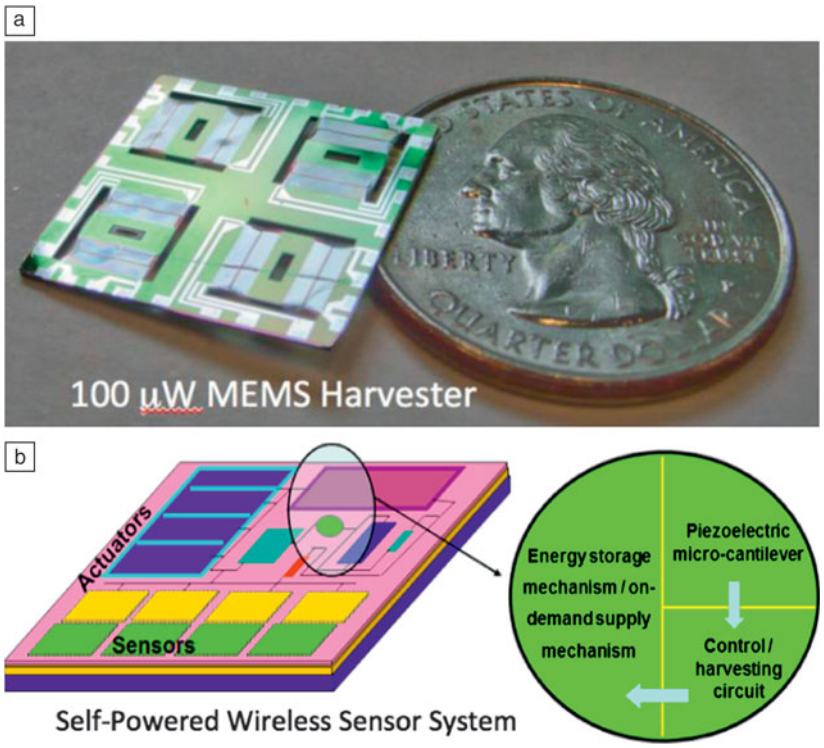

Figure 9. Examples of piezoelectric energy harvesting systems. (a) Photograph of a compact piezoelectric microelectromechanical system (MEMS) energy harvesting device, which is about the size of a US quarter ($0.25) coin. A doubly clamped beam acts as a frequency locked loop, resulting in wide bandwidth, non-linear resonance. (b) Schematic of on-chip architecture for a self-powered wireless sensor network system. Robust self-powering can be achieved by utilizing all environmental energy resources, as well as dual purpose sensors and actuators, which also act as energy harvesters.[87]

The article by Kim et al. in this issue demonstrates the promise of piezoelectric technology as a local power source able to capture available mechanical energy from the environment. One approach to enhance the output power at a fixed size of a device is to increase the figure of merit for energy from piezoelectric thin films. Epitaxial and strong-oriented piezoelectric films are being developed for this purpose. Another approach is more efficient mechanical design of cantilever resonator structures. For example, Hajati et al. have recently demonstrated a monolithic, MEMS-based, non-linear, resonant piezoelectric micro-energy harvester.[72] Significant improvements, greater than an order of magnitude in both power bandwidth and normalized power density, were demonstrated compared to previously reported devices.

More typically, however, piezoelectric MEMS range from a few tens of microns to a few mm in the lateral dimension. A wide array of devices, including filters, resonators, accelerometers, pumps, switches, optical scanners, and acoustic sources, have been fabricated, as discussed in a number of review articles.[24–27] At this size scale, sensors and actuators are generally prepared either by surface or bulk micromachining of devices. In many cases, the resulting structures operate in a bending mode (e.g., with a piezoelectric elastically coupled to a passive layer to produce a unimorph). This geometry enables mechanical amplification of displacements for actuators, as well as stress amplification in sensing devices. In this issue, the articles by Piazza et al., Pulskamp et al., Kim et al., and Funakubo et al. review a few of the active research areas in piezoelectric MEMS at this size scale.

Resonators and filters

The article by Piazza et al. summarizes the most commercially advanced area of piezoelectric MEMS: AlN-based devices for filters and resonators (see **Figure 10**). Thin-film bulk acoustic resonators are now ubiquitous in mobile communication devices and have resulted in an over three orders of magnitude decrease in the volume required for the duplexer (the component that allows both transmit and receive signals to share an antenna while retaining signal fidelity) since 2000. This is one of the key components that has enabled the reduction in the form factor of cellular telephones relative to the clunky devices prior to the turn of the century. More than 10^9 AlN-based acoustic resonator devices are sold per year. Essential to their operation is growth of highly textured wurtzite-structured films with very well defined thicknesses. Research is now advancing AlN-based piezoelectric MEMS in numerous areas, including high sensitivity sensors and energy harvesting devices. In both cases, the low permittivity of AlN relative to ferroelectric materials such as PZT or PMN-PT is advantageous in producing large voltages for small excitations. AlN-based piezoelectric MEMS are also one of the enabling technologies for reconfigurable radios,[73] which could revolutionize future communication devices.

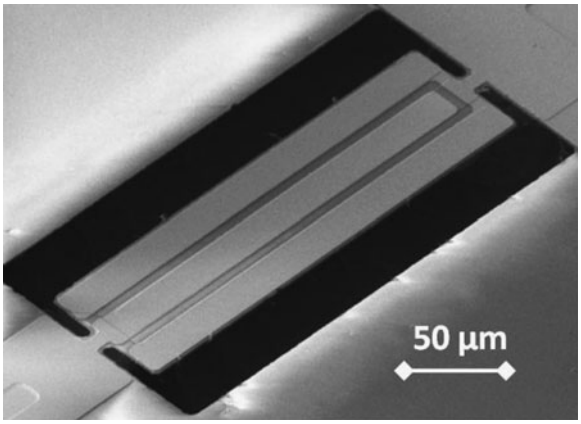

Figure 10. AlN contour-mode resonator. Image courtesy of G. Piazza.

https://doi.org/10.1557/mrs.2012.273 Published online by Cambridge University Press

Piezoelectric inkjet printing

Since the first patent by Steven Zoltan[74] of the Clevite Company in 1976, and the first commercial product by Siemens in 1977, most commercial and industrial piezoelectric inkjet printers have used an actuator in an ink-filled chamber behind each nozzle. Compared with alternative actuation methods (e.g., thermal, electrostatic), piezoelectric inkjet printers are ink-independent and able to work at elevated temperatures. These advantages show the potential adaptability of piezoelectric inkjet technology to alternative applications, such as printed electronics, printed biosensors, and 3D printing. However, current utilization of bulk PZT as the piezoelectric actuator material poses a significant manufacturing challenge. The bulk PZT is not compatible with wafer-scale batch fabrication processes. Consequently, the costs of conventional piezoelectric (bulk-based) print heads are prohibitive for dense arrays. Since the early 1990s, piezoelectric PZT thin films have been studied intensively, and improved preparation methods have been developed at the laboratory scale. New products, such as piezoelectric MEMS print heads, are envisaged, and technology is currently being developed for the industrial-scale integration of piezoelectric thin films into MEMS.[31,75] **Figure 11** shows a process of epitaxial piezoelectric thin films to ink droplet creation by using an epitaxial piezoelectric of $Pb(Zr,Ti)O_3$ thin films. Prospects for future development of this technology are discussed in the article by Funakubo et al. in this issue.

Insect robotics and more

The article by Pulskamp et al. highlights the state-of-the-art in PZT-based MEMS devices, as well as the diversity of the devices that are enabled by high strain piezoelectric films. **Figure 12** shows typical examples. Large-scale motion is achieved using the mechanical amplification implicit in bending structures via the $e_{31,f}$ coefficient. This approach allows modest electric field-induced in-plane stresses to be amplified into large out-of-plane (or even in-plane) displacements at low driving voltages (~1–20 V, typically). As a result, structures that are only approximately a hundred microns in lateral dimensions can produce deflections of tens of microns. The application of piezoelectrics films to ultrasonic motors and flapping wing structures are discussed. The use of thin-film PZT to achieve high performance and low-voltage radio frequency (RF) MEMS switches, ultralow power consumption nanomechanical logic circuits, and high coupling and low loss resonators, filters, and transformers are reviewed. It is intriguing that comparatively mechanically lossy materials such as PZT can be utilized in resonators, providing the mechanical energy is predominantly confined in the passive elastic layer.

Other challenges are emerging as electromechanical systems move to the nanoscale (NEMS) with increasing integration density, while requiring faster and larger relative motion range. NEMS have begun to find applications in many electrical and optical communications systems where fast, flexible switching or filtering is required. Examples include high frequency RF filters and optical arrays.[76–80] Recent advances in the integration of piezoelectric materials to make *active* electromechanical systems enable large forces at small drive voltages with fast actuation, high sensitivity sensors for ultrasmall mechanical displacements, accurate electrically induced displacements at high integration densities, reduced voltage burden on the integrated control electronics, and decreased MEMS and NEMS complexity.

Piezotronic NEMS for beyond-CMOS logic

The article by Newns et al. in this issue details a revolutionary application of piezoelectric NEMS. Recently, the drive toward reducing power in CMOS electronics has prompted research on scalable NEMS for switching applications in computation.[81] Piezoelectric MEMS and NEMS enable lower voltage versions of those devices than their electrostatic analogs. They show that piezoelectric NEMS offers a route to increasing computer clock speeds for the first time in nearly a decade, while requiring substantially lower power for operation. Fundamentally, the device operates by using a piston-like motion of a piezoelectric to compress a strongly piezoresistive material. Piezotronic devices offer the possibility of both logic and memory functionalities and would overcome physical limitations in the scaling of CMOS electronics.

Outlook and future opportunities

The articles in this issue paint a bright future for the ongoing development of piezoelectric thin films by increasing piezoelectric response, advances in integration, and application as

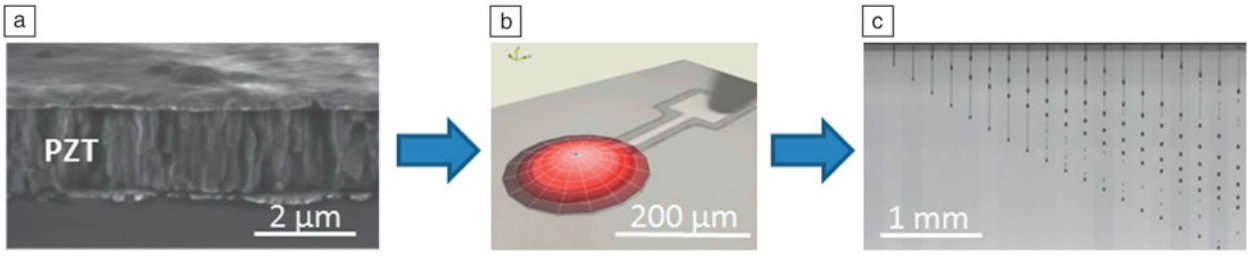

Figure 11. From epitaxial piezoelectric thin films to ink droplet creation. (a) Cross-section scanning electron micrograph of a $Pb(Zr,Ti)O_3$ (PZT) thin film, (b) optical micrograph of piezoelectric actuated microelectromechanical membrane, and (c) ink droplet jets.

https://doi.org/10.1557/mrs.2012.273 Published online by Cambridge University Press

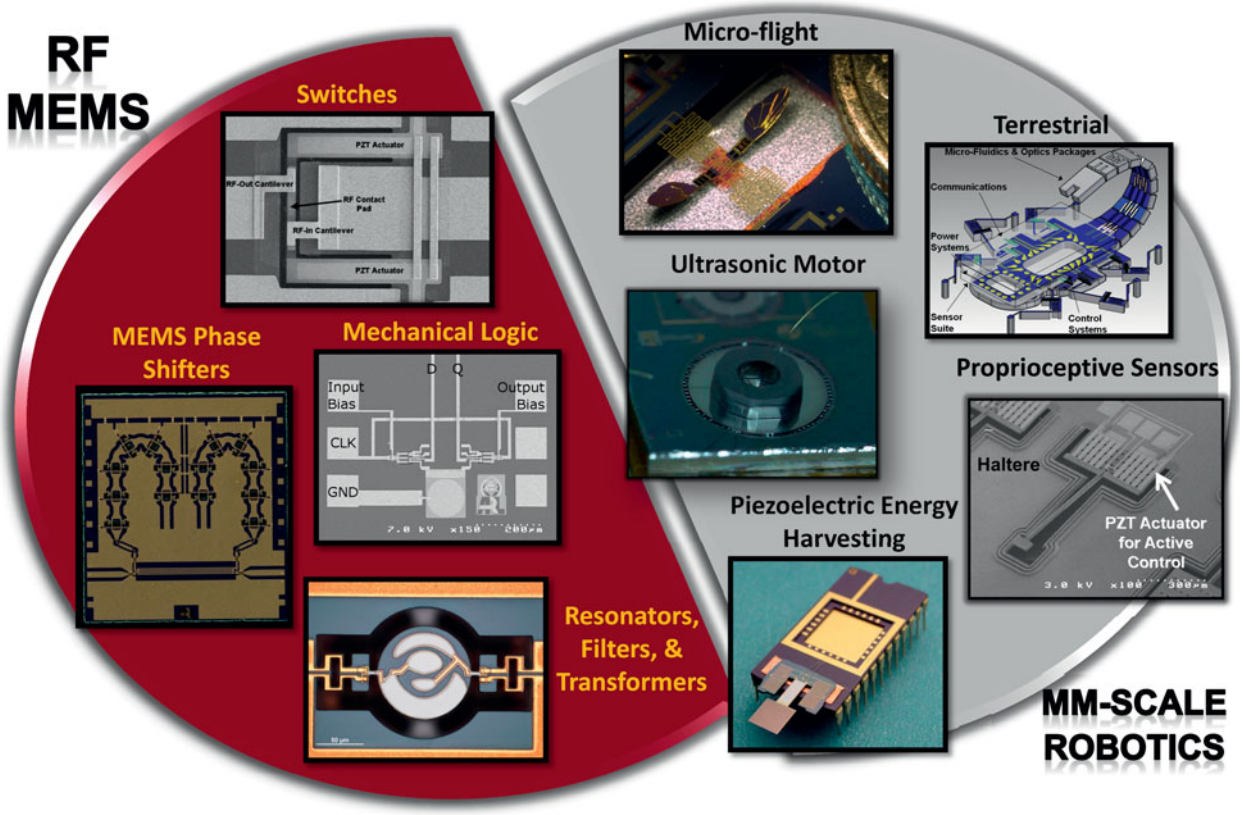

Figure 12. Montage of piezoelectric microelectromechanical (MEMS) devices. For the motor, the piezo MEMS stator is 3 mm in diameter, and the Si rotor is 2 mm in diameter. The switch uses a PZT actuator with a length of 125 microns. The phase shifter designed for 10 GHz operation has an overall dimension of 5.0 mm × 5.5 mm. The dual-wing micro wing structure was designed with 2 mm length wings. The piezoelectric energy harvester uses a 5-mm-long PZT thin-film cantilever that attached to a 5 mm × 5 mm proof mass. Image courtesy of Jeffrey S. Pulskamp and Ronald G. Polcawich, US Army Research Laboratory. Note: RF, radio frequency; PZT, $Pb(Zr,Ti)O_3$; CLK, clock; GND, ground.

piezoelectric sensors, actuators, resonators, energy harvesters, and other novel devices. These accomplishments have been driven by advances in thin-film growth and by design improvements that take advantage of the unique characteristics of thin-film piezoelectrics. Future challenges include the development of higher response thin-film piezoelectrics, refined control of surface roughness, and the exploration of nanoscale piezoelectric device behavior where aspects such as flexoelectric effects are likely to provide new opportunities.

One vital strength of the field of piezoelectric-microelectromechanical systems (MEMS) is its highly interdisciplinary nature. This is a field where materials research is critical in advancing science and technology for both physical and biological sciences. As piezoelectric materials improve, and the integration of diverse form and function becomes manufacturable, the contribution of materials research becomes essential to continued scientific and technological progress. This is also a research area in which theoretical research plays an important role. Computational approaches such as first-principle calculations, thermodynamic calculations, and phase-field simulations methods further aid the study of interplay between strain, substrate clamping, defects, domain structures, size, and piezoelectric properties in piezoelectric mechanical systems.[82–86] The field of piezo-MEMS will expand to next-generation electronic, medical, and energy devices enabled by new, higher performance integrated piezoelectric thin-film materials.

Acknowledgments

Chang-Beom Eom gratefully acknowledges support from the National Science Foundation (grant no. ECCS-0708759) and the David & Lucile Packard Fellowship. Susan Trolier-McKinstry gratefully acknowledges support from a National Security Science and Engineering Faculty Fellowship, as well as the National Science Foundation for a Nanoscience Engineering Research Center program (EEC-1160483).

References

1. S.E. Park, T.R. Shrout, *J. Appl. Phys.* **82**, 1804 (1997).
2. T. Takenaka, H. Nagata, *J. Eur. Ceram. Soc.* **25**, 2693 (2005).
3. K.L. Ekinci, M.L. Roukes, *Rev. Sci. Instrum.* **76**, 061101 (2005).
4. Y.T. Yang, K.L. Ekinci, X.M.H. Huang, L.M. Schiavone, M.L. Roukes, C.A. Zorman, M. Mehregany, *Appl. Phys. Lett.* **78**, 162 (2001).
5. A.B. Hutchinson, P.A. Truitt, K.C. Schwab, L. Sekaric, J.M. Parpia, H.G. Craighead, J.E. Butler, *Appl. Phys. Lett.* **84**, 972 (2004).
6. D. Lopez, M.E. Simon, F. Pardo, V. Aksyuk, F. Klemens, R. Cirelli, D.T. Neilson, H. Shea, T. Sorsch, E. Ferry, O. Nalamasu, P.L. Gammel, *2002 IEEE/LEOS International Conference on Optical MEMS* (2002), p. 211.

https://doi.org/10.1557/mrs.2012.273 Published online by Cambridge University Press

7. V.A. Aksyuk, M.E. Simon, F. Pardo, S. Arney, D. Lopez, A. Villanueva, *Solid-State Sensor and Actuator Workshop* (Hilton Head Island, SC, 2002), pp. 1–6.
8. D.M. Marom, D.T. Neilson, D.S. Greywall, C.S. Pai, N.R. Basavanhally, V. Aksyuk, D. Lopez, F. Pardo, M.E. Simon, Y. Low, P. Kolodner, C.A. Bolle, *IEEE J. Lightwave Technol.* **23** (1), 1620 (2005).
9. V.A. Aksyuk, F. Pardo, D. Carr, D. Greywall, H.B. Chan, M.E. Simon, A. Gasparyan, H. Shea, V. Lifton, C. Bolle, S. Arney, R. Frahm, M. Paczkowski, M. Haueis, R. Ryf, D.T. Neilson, J. Kim, C.R. Giles, D. Bishop, *J. Lightwave Technol.* **21** (3), 634 (2003).
10. S. Trolier-McKinstry, P. Muralt, *J. Electroceram.* **12** (1–2), 7 (2004).
11. D. Damjanovic, *Appl. Phys. Lett.* **97** (6), 062906 (2010).
12. V. Cimallam, J. Pezoldt, O. Armbacher, *J. Phys. D: Appl. Phys.* **40** (20), 6386 (2007).
13. K.M. Lakin, G.R. Kline, K.T. McCarron, *IEEE Trans. Microwave Theory Tech.* **41** (12), 2139 (1993).
14. R. Ruby, P. Bradley, J.D. Larson, Y. Oshmyansky, *Electron. Lett.* **35** (10), 794 (1999).
15. S. Roundy, P.K. Wright, J. Rabaey, *Comp. Commun.* **26** (11), 1131 (2003).
16. A. Erturk, D.L. Inman, *Piezoelectric Energy Harvesting* (Wiley, New York, 2011).
17. K.A. Cook-Chennault, N. Thambi, A.M. Sastry, *Smart Mater. Struct.* **17** (4), 043001 (2008).
18. N.E. DuToit, B.L. Wardle, *AIAA J.* **45** (5), 1126 (2007).
19. J.S. Yun, S.N. Patel, M.S. Reynolds, G.D. Abowd, *IEEE Trans. Mob. Comput.* **10**, 669 (2011).
20. L. Moro, D. Benasciutti, *Smart Mater. Struct.* **19**, 115011 (2010).
21. T. von Buren, P.D. Mitcheson, T.C. Green, E.M. Yeatman, A.S. Holmes, G. Troster, *IEEE Sens. J.* **6**, 28 (2006).
22. M.A. Karami, D.J. Inman, *Appl. Phys. Lett.* **100** (4), 042901 (2012).
23. D.D. Fong, G.B. Stephenson, S.K. Streiffer, J.A. Eastman, O. Auciello, P.H. Fuoss, C. Thompson, *Science* **304** (5677), 1650 (2004).
24. D.L. Polla, L.F. Francis, *Annu. Rev. Mater. Sci.* **28**, 563 (1998).
25. P. Muralt, R.G. Polcawich, S. Trolier-McKinstry, *MRS Bull.* **34** (9), 658 (2009).
26. S. Trolier-McKinstry, F. Griggio, C. Yaeger, P. Jousse, D. Zhao, S.S.N. Bharadwaja, T.N. Jackson, S. Jesse, S.V. Kalinin, K. Wasa, *IEEE Trans. Ultrason. Ferroelectr. Freq. Control* **58** (9), 1782 (2011).
27. S.A. Wilson, R.P.J. Jourdain, Q. Zhang, R.A. Dorey, C.R. Bowen, M. Willander, Q.U. Wahab, M.A.H. Safaa, O. Nur, E. Quandt, C. Johansson, E. Pagounis, M. Kohl, J. Matovic, B. Samel, W. van der Wijngaart, E.W.H. Jager, D. Carlsson, Z. Djinovic, M. Wegener, C. Moldovan, R. Iosub, E. Abad, M. Wendlandt, C. Rusu, K. Persson, *Mater. Sci. Eng. Rep.* **56** (1–6), 1 (2007).
28. G.L. Smith, J.S. Pulskamp, L.M. Sanchez, D.M. Potrepka, R.M. Proie, T.G. Ivanov, R.Q. Rudy, W.D. Nothwang, S.S. Bedair, C.D. Meyer, R. Polcawich, *J. Am. Ceram. Soc.* **95** (6), 1777 (2012).
29. S.J. Gross, S. Tadigadapa, T.N. Jackson, S. Trolier-McKinstry, Q.Q. Zhang *Appl. Phys. Lett.* **83**, 174 (2003).
30. A.N. Cleland, M. Pophristic, I. Ferguson, *Appl. Phys. Lett.* **79**, 2070 (2001).
31. E. Fujii, R. Takayama, K. Nomura, A. Murata, T. Hirasawa, A. Tomozawa, S. Fujii, T. Kamada, T.H. Torii, *IEEE Trans. Ultrason. Ferroelectr. Freq. Control* **54** (12), 2431 (2007).
32. J.F. Scott, C.A. Paz de Araujo, *Science* **246**, 1400 (1989).
33. O. Auciello, J.F. Scott, R. Ramesh, *Phys. Ferroelectr. Memories* **51**, 22 (1998).
34. R.E. Newnham, *MRS Bull.* **22** (5), 20 (1995).
35. X.L. Zhang, Z.X. Chen, L.E. Cross, W.A. Schulze, *J. Mater. Sci.* **18** (4), 968 (1983).
36. H.X. Fu, R.E. Cohen, *Nature* **403** (6767), 281 (2000).
37. D. Damjanovic, *Appl. Phys. Lett.* **97** (6), 062906 (2010).
38. A. Pramanick, D. Damjanovic, J. Daniels, J.C. Nino, J.L. Jones, *J. Am. Ceram. Soc.* **94** (2), 293 (2011).
39. B. Xu, Y. Ye, L.E. Cross, J.J. Bernstein, R. Miller, *Appl. Phys. Lett.* **74**, 3549 (1999).
40. E.K. Hong, S. Trolier-McKinstry, R.L. Smith, S.V. Krishnaswamy, C.B. Freidhoff, *J. Microelectromech. Syst.* **15**, (4), 832 (2006).
41. S.B. Desu, D.P. Vijay, X. Zhang, B.P. He, *Appl. Phys. Lett.* **69**, 1719 (1996).
42. S.K. Streiffer, C. Basceri, C.B. Parker, S.E. Lash, A.I. Kingon, *J. Appl. Phys.* **86**, 4565 (1999).
43. C.B. Eom, R.B. van Dover, J.M. Phillips, D.J. Werder, J.H. Marshall, C.H. Chen, R.J. Cava, R.M. Fleming, D.K. Fork, *Appl. Phys. Lett.* **63**, 2570 (1993).
44. T. Tybell, C.H. Ahn, J.M. Triscone, *Appl. Phys. Lett.* **75**, 856 (1999).
45. P. Muralt, *J. Am. Ceram. Soc.* **91**, 1385 (2008); doi: 10.1111/j.1551-2916.2008.02421.x.
46. H. Lu, X. Liu, D.J. Kim, A. Stamm, J.D. Burton, P. Lukashev, C.W. Bark, D.A. Felker, C.M. Folkman, X. Pan, M.S. Rzchowski, C.-B. Eom, E.Y. Tsymbal, A. Gruverman, *Adv. Mater.* **24**, 1209 (2012).
47. M.K. Lee, C.B. Eom, W. Tian, X.Q. Pan, M.C. Smoak, F. Tsui, J.J. Krajewski, *Appl. Phys. Lett.* **77**, 364 (2000).
48. J.M. Triscone, O. Fischer, O. Brunner, L. Antognazza, A.D. Kent, M.G. Karkut, *Phys. Rev. Lett.* **64**, 804 (1990).
49. J.C. Jiang, X.Q. Pan, W. Tian, C.D. Theis, D.G. Schlom, *Appl. Phys. Lett.* **74**, 2851 (1999).
50. M. Dekkers, M.D. Nguyen, R. Steenwelle, P.M. te Riele, D.H.A. Blank, G. Rijnders *Appl. Phys. Lett.* **95**, 012902 (2009).
51. T.M. Shaw, S. Trolier-McKinstry, P.C. McIntyre, *Annu. Rev. Mater. Sci.* **30**, 263 (2000).
52. Y.L. Li, S. Choudhury, Z.K. Liu, L.Q. Chen, *Appl. Phys. Lett.* **83**, 1608 (2003).
53. K.J. Choi, M. Biegalski, Y.L. Li, A. Sharan, J. Schubert, R. Uecker, P. Reiche, Y.B. Chen, X.Q. Pan, V. Gopalan, L.-Q. Chen, D.G. Schlom, C.B. Eom, *Science* **306**, 1005 (2004).
54. J.H. Haeni, P. Irvin, W. Chang, R. Uecker, P. Reiche, Y.L. Li, S. Choudhury, W. Tian, M.E. Hawley, B. Craigo, A.K. Tagantsev, X.Q. Pan, S.K. Streiffer, L.Q. Chen, S.W. Kirchoefer, J. Levy, D.G. Schlom, *Nature* **430**, 758 (2004).
55. D.G. Schlom, L.Q. Chen, C.-B. Eom, K.M. Rabe, S.K. Streiffer, J.M. Triscone, *Annu. Rev. Mater. Res.* **237**, 589 (2007).
56. J.X. Zhang, B. Xiang, Q. He, J. Seidel, R.J. Zeches, P. Yu, S.Y. Yang, C.H. Wang, Y.-H. Chu, L.W. Martin, A.M. Minor, R. Ramesh, *Nat. Nanotechnol.* **6**, 98 (2011).
57. A.K. Sharma, J. Narayan, C. Jin, A. Kvit, S. Chattopadhyay, C. Lee, *Appl. Phys. Lett.* **76**, 1458 (2000).
58. R.A. McKee, F.J. Walker, M.F. Chisholm, *Phys. Rev. Lett.* **81**, 3014 (1998).
59. J. Lettieri, *Critical Issues of Complex, Epitaxial Oxide Growth and Integration with Silicon by Molecular Beam Epitaxy* (Pennsylvania State University, University Park, 2002); http://etda.libraries.psu.edu/theses/approved/WorldWideIndex/ETD-202/index.html.
60. J.W. Reiner, A.M. Kolpak, Y. Segal, K.F. Garrity, S. Ismail-Beigi, C.H. Ahn, F.J. Walker, *Adv. Mater.* **22**, 2919 (2010).
61. R. Ramesh, A. Inam, W.K. Chan, B. Wilkens, K. Myers, K. Remschning, D.L. Hart, J.M. Tarascon, *Science* **252**, 944 (1991).
62. C.B. Eom, R.J. Cava, R.M. Fleming, J.M. Phillips, R.B. van Dover, J.H. Marshall, J.W.P. Hsu, J.J. Krajewski, W.F. Peck Jr., *Science* **258**, 1766 (1992).
63. D.S. Paik, S.E. Park, S. Wda, S.F. Liu, T.R. Shrout, *J. Appl. Phys.* **85**, 1080 (1999).
64. C.B. Eom, J.Z. Sun, K. Yamamoto, A.F. Marshall, K.E. Luther, T.H. Geballe, S.S. Laderman, *Appl. Phys. Lett.* **55**, 595 (1989).
65. S.H. Baek, J. Park, D.M. Kim, V. Aksyuk, R.R. Das, S.D. Bu, D.A. Felker, J. Lettieri, V. Vaithyanathan, S.S.N. Bharadwaja, N. Bassiri-Gharb, Y.B. Chen, H.P. Sun, C.M. Folkman, H.W. Jang, D.J. Kreft, S.K. Streiffer, R. Ramesh, X.Q. Pan, S. Trolier-McKinstry, D.G. Schlom, M.S. Rzchowski, R.H. Blick, C.B. Eom, *Science* **334**, 958 (2011).
66. S.A. Bhave, R.T. Howe, *Proc. 13th Int. Conf. on Solid-State Sensors, Actuators and Microsystems* (2005), p. 2139.
67. E.-H. Yang, Y. Hishinuma, J.-G. Cheng, S. Trolier-McKinstry, E. Bloemhof, B.M. Levine, *J. Microelectromech. Syst.* **15** (5), 1214 (2006).
68. J.L. Fanson, *MRS Proc.* **360**, 109 (1995).
69. C.L. Him, P.D. Dean, S.R. Winzer, *Proc. SPIE* **3985**, 394 (2000).
70. R.A. Windhorst, R.A. Cameron, R.J. Brissenden, M.S. Elvis, G. Fabbiano, P. Gorenstein, P.B. Reid, D.A. Schwartz, M.W. Bautz, E. Figueroa-Feliciano, R. Petre, N.E. White, W.W. Zhang, *New Astron. Rev.* **50**, 121 (2006).
71. V. Cotroneo, W.M. Davis, P.B. Reid, D.A. Schwartz, S. Trolier-McKinstry, R.H.T. Wilke, *Proc. SPIE* **8147**, 81471R (2011).
72. A. Hajati, S.G. Kim, *Appl. Phys. Lett.* **99**, 083105 (2011).
73. C.J. Zuo, N. Sinha, G. Piazza, *Sens. Act. A.* **160** (1–2), 132 (2010).
74. S. Zlotan, US Patent 3965376 (June 22, 1976).
75. http://global.epson.com/innovation/printing_technology/micro_piezo_technology/future.
76. M.L. Roukes, *Phys. World* **14**, 25 (2001).
77. H.G. Craighead, *Science* **290**, 1532 (2000).
78. C.T.-C. Nguyen, *IEEE Trans. Microwave Theory Tech.* **47**, 1486 (1999).
79. R.H. Blick, A. Erbe, L. Pescini, A. Kraus, D.V. Scheible, F.W. Beil, E.M. Höhberger, A. Hoerner, J. Kirschbaum, H. Lorenz, J.P. Kotthaus, *J. Phys. Condens. Matter* **14**, R905 (2002).
80. A.N. Cleland, *Foundations of Nanomechanics—From Solid-State Theory to Device Applications* (Springer-Verlag, Berlin, 2003).
81. K. Akarvardar, D. Elata, R. Parsa, G.C. Wan, K. Yoo, J. Provine, P. Peurnans, R.T. Howe, H.S.P. Wong, *IEEE IEDM* (2007), p. 299.
82. L. Bellaiche, D. Vanderbilt, *Phys. Rev. Lett.* **83**, 1347 (1999).
83. G. Saghi-Szabo, R.E. Cohen, H. Krakauer, *Phys. Rev. Lett.* **80**, 4321 (1998).
84. O.Y. Jun, R. Ramesh, A.L. Roytburd, *Appl. Surf. Sci.* **252**, 3394 (2006).
85. Y. Cao, G. Sheng, J.X. Zhang, S. Choudhury, Y.L. Li, C.A. Randall, L.Q. Chen, *Appl. Phys. Lett.* **97**, 252904 (2010).
86. L.Q. Chen, *J. Am. Ceram. Soc.* **91**, 1835 (2008).
87. H. Kim, S. Priya, H. Stephanou, K. Uchino, *IEEE Trans. Ultrason. Ferroelectr. Freq. Control* **54**, 1851 (2007). □

https://doi.org/10.1557/mrs.2012.273 Published online by Cambridge University Press